Liquid−Liquid−Vapor, Liquid−Liquid, and Liquid−Vapor Phase Transitions in Aqueous *n*-Hexane Mixtures from Isochoric Heat Capacity Measurements

Ibragimkhan K. Kamilov, Gennadii V. Stepanov, Ilmutdin M. Abdulagatov,* Anvar R. Rasulov, and Elena I. Milikhina

Institute of Physics of the Daghestan Scientific Center of the Russian Academy of Sciences, Yaragskogo str. 94, Makhachkala, Dagestan, Russia 367003

The constant volume and constant composition heat capacity C_{VX} data for aqueous *n*-hexane mixtures are reported for seven compositions, (0.6146, 0.7965, 0.9349, 0.9775, 0.9858, 0.9892, and 0.9940) mol fraction of *n*-hexane, along seven near-critical isochores between 259.34 and 312.50 kg·m^{-3} in the temperature range from 463 to 522 K at pressures up to 6 MPa. All of these isochores display two features in the heat capacity as a function of temperature: the first peak appears when one of the liquid phases disappears, and the second peak appears when the vapor or liquid phase disappears. These features are interpreted in terms of the liquid−liquid−vapor, liquid−liquid, and liquid−vapor phase diagram, and their consistency is shown with earlier *PTx* measurements on the three-phase (L-L-G) boundary. Measurements of the isochoric heat capacity (C_VVTx) of water + *n*-hexane mixtures were made in a spherical high-temperature, high-pressure nearly constant volume adiabatic calorimeter. The calorimeter was also used as a constant-volume piezometer to measure the *PVTx* properties. The uncertainties of the measurements are as follows: isochoric heat capacity, 1.0−1.5%; density, 0.1%; temperature, 10 mK; and pressure, 0.05%. The method of quasi-static thermograms was used to precisely measure the liquid−liquid−gas (L-L-G), liquid−liquid (L-L), and liquid−gas (L-G) phase transition temperatures at each fixed density, with an uncertainty of 0.02 K. New saturated densities and pressures are presented on the (L-L-G) and (L-G) phase boundaries. The values of temperature, pressure, and density of the upper critical end point (UCEP) in the water + *n*-hexane mixture were determined from the measurements. Results for the UCEP (T_{UCEP} = 495.82 K; P_{UCEP} = 5.25 MPa; ρ_{UCEP} = 259.9 kg·m^{-3}) are in good agreement with the values reported by other authors. For the first time the temperature-dependent behavior of C_{VX} near the UCEP is reported.

Introduction

The thermodynamic behavior of mixtures in the vicinity of the critical point of one of the components has considerable practical and theoretical importance.[1−6] Near-critical and supercritical water (SCW), like carbon dioxide, has been proposed as an environmentally acceptable solvent or reaction medium for a number of technological applications.[7−14] In particular, the thermodynamic properties of hydrocarbons in water at high temperatures and high pressures is of considerable interest in petroleum engineering and chemistry (reservoir fluids, enhanced oil recovery), environmental protection (removal of hydrocarbons from wastewater, fate of hydrocarbons in geological fluids), organic chemistry, geology and mineralogy, new separation techniques, biological degradations without char formation, etc. Fundamental understanding of some of these technologically important applications of near-critical and supercritical mixtures might be substantially improved through a knowledge of the solvation structures around solutes dissolved in SCW. SCW has emerged as an important medium for carrying out chemical reactions,[13−18] especially in the area of toxic waste destruction.[8−14] Organic materials are oxidized in SCW to yield environmentally clean products such as water, carbon dioxide, and other small molecules.[8−14] SCW extraction has been used by Hawthorne et al.[19] and Yang et al.[20] to remove organic pollutants from environmental solids, such as soils, sediments, and air particulates. Little is known about the reaction mechanism and the molecular picture of solvation under supercritical conditions. SCW is receiving increased interest as an alternative to organic solvents. In contrast to the low polarity of supercritical CO_2, water is too polar to efficiently dissolve organic materials. Low-polarity organics do not have high water solubilities at ambient conditions, whereas SCW has a much lower dielectric constant and therefore is an extremely effective solvent for organics.[20−25] SCW can solubilize most nonpolar organic compounds including hydrocarbons. The solubility of organics increases considerably with rising temperature, especially in the vicinity of the critical point of pure water. Above 350 °C and 25 MPa, organic materials such as benzene, toluene, and *n*-alkanes are completely miscible with water. Enhanced solvent clustering in nonpolar supercritcal fluids has been found from spectroscopic studies.[26−31] Gao[32] used Monte Carlo simulations to examine the hydrophobic effect of organic molecules (benzene) in SCW. Molecular dynamics and Monte Carlo studies[33−38] of solute−solvent microstructure in aqueous solutions at supercritical condition yield valuable insights into solute−solvent interactions in SCW.

* Address correspondence to this author at the National Institute of Standards and Technology, 325 Broadway, Boulder, CO 80305 [fax (303) 497-5224; e-mail ilmutdin@boulder.nist.gov].

10.1021/je010136s CCC: $20.00
Published on Web 09/25/2001

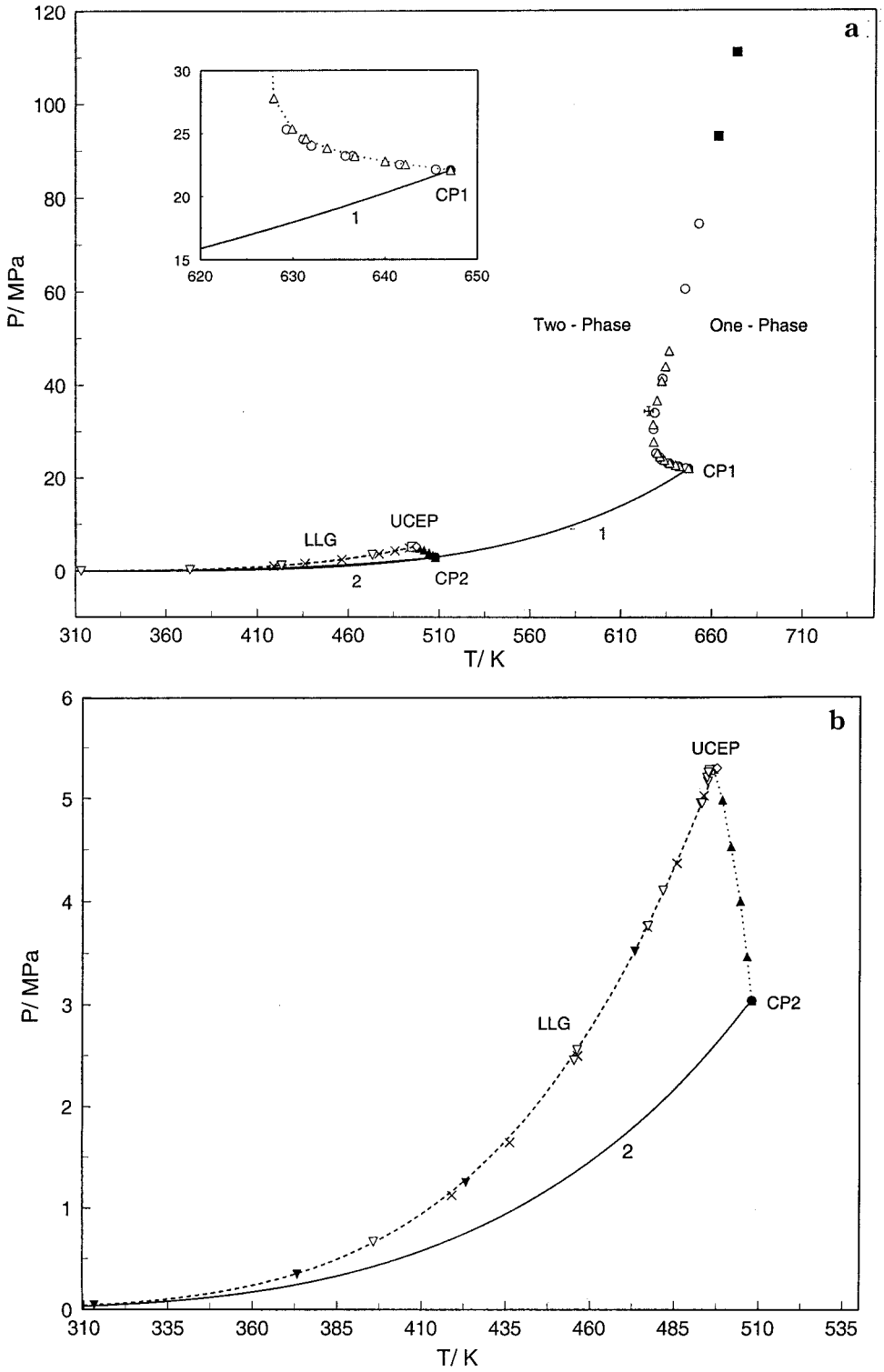

Figure 1. Pressure−temperature phase diagram for water + *n*-hexane mixture: CP1, critical point of pure water;[81] CP2, critical point of pure *n*-hexane;[78] 1, vapor pressure curve for pure water calculated from the IAPWS-95 formulation;[73] 2, vapor pressure curve for pure *n*-hexane calculated from Span's multiparametric EOS;[74] dashed line, three-phase (L-L-G) equilibrium curve (eq 1, Tsonopoulos and Wilson[55]); dotted line, critical curve; ▲, Brunner;[48] ◇, Roof;[80] ○, De Loos et al.;[46] ■, Yiling et al.;[47] □, Scheffer;[79] ×, Brunner;[48] △, Brunner;[48] ▽, this work; ▼, Tsonopoulos and Wilson;[55] Maltese cross, Connolly.[22]

Design and control of systems for supercritical fluid extraction require pure-component and mixture thermodynamic properties and molecular-based understanding of the mechanism underlying the supercritical solubility enhancement. Efficient utilization of the possibilities offered by supercritical fluid solubility requires an accurate and detailed knowledge of the fluid thermodynamic properties, particularly the C_VVTx relationship of the near-critical and supercritical mixtures, and properties on the two- [liquid−liquid (L-L), liquid−gas (L-G)] and three-phase [liquid−liquid−gas (L-L-G)] curves. Isochoric heat capacity measurements are very sensitive to accurate measurements of the phase boundary for complicated mixtures such as water + hydrocarbons. C_VVTx measurements improve our understanding of many important phenomena taking place near phase transitions and critical points.

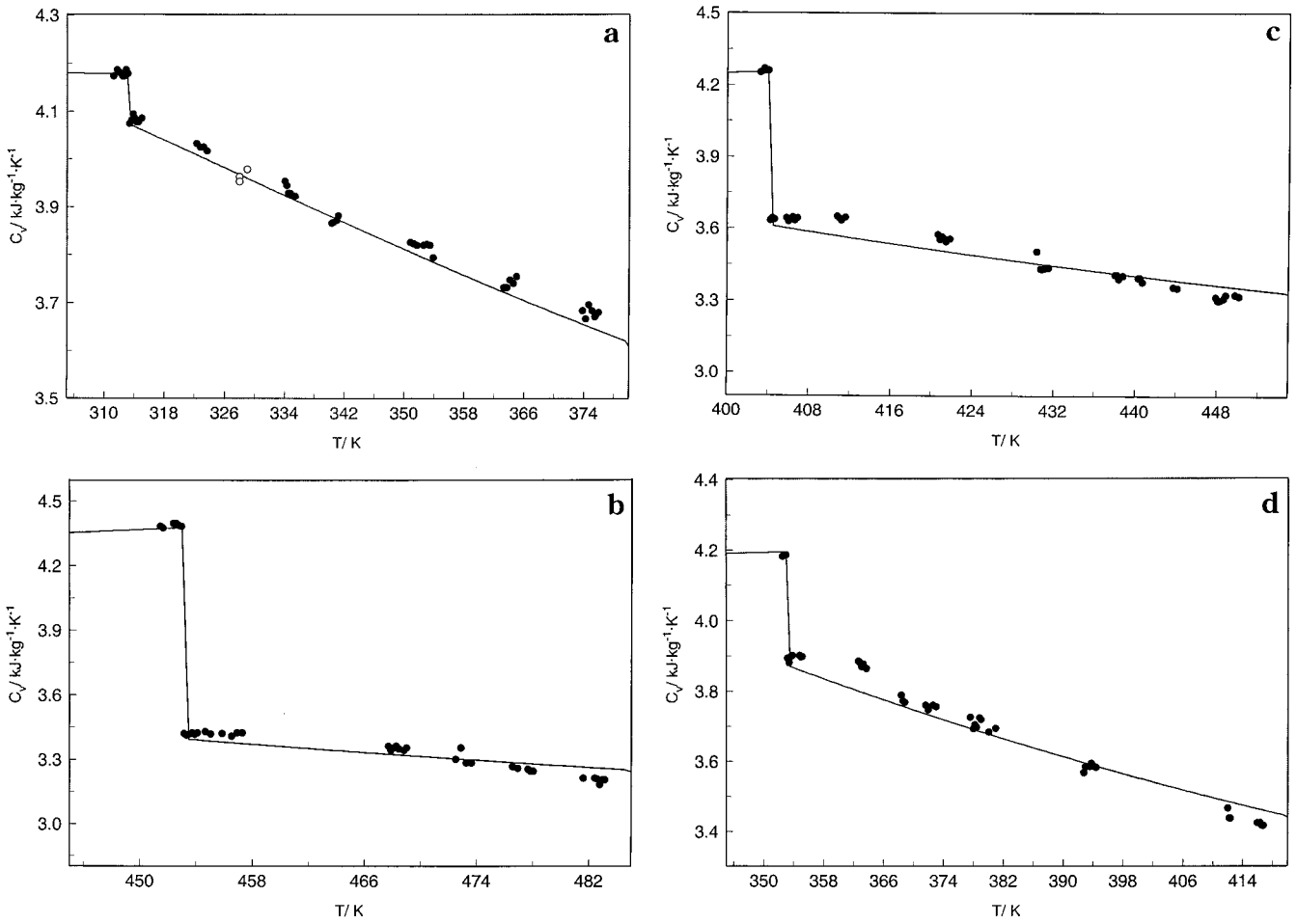

Figure 2. Experimental heat capacities of pure water (●, Amirkhanov et al.,[63] and ○, Magee et al.[75]) as a function of temperature along liquid isochores together with values calculated from the IAPWS-95 formulation[73] (solid lines): (a) 992.16 kg·m^{-3}; (b) 886.92 kg·m^{-3}; (c) 933.97 kg·m^{-3}; (d) 971.82 kg·m^{-3}.

The purpose of this paper is to obtain new experimental C_VVTx data and (L-L-G, L-L, and L-G) phase transition parameters ($PVTx$) for water + *n*-hexane mixtures in the critical region. Measurements are to be carried out in the vicinity of the lower branch of the critical curve for water + *n*-hexane mixtures using the same apparatus as used in our previous papers.[39−44] In the present paper we are continuing our previous investigations[40−42] of the C_VVTx properties of water + *n*-hexane mixtures with a high temperature and high pressure and nearly constant volume adiabatic calorimeter. Previously, C_VVTx data for water + *n*-hexane mixtures were reported by Kamilov et al.[40,41] and Stepanov et al.[42] Kamilov et al.[40] reported C_VVTx and $PVTx$ data for water + *n*-hexane mixtures at seven compositions, (0.385, 0.655, 0.699, 0.744, 0.753, 0.8, and 0.879) mol fraction of C_6H_{14}, and at temperatures from 365 to 622 K. Pressures ranged from 0.5 to 24 MPa and densities from 191.4 to 416.7 kg·m^{-3}. Our new experimental C_VVTx data for water + *n*-hexane mixtures in the immediate vicinity of (L-L-G, L-L, and L-G) phase transition points are very important for stringent testing of phase boundary calculations for this system.

A number of phase equilibrium studies have been made on water + *n*-hexane mixtures.[45−48] All of the measurements were performed at temperatures up to the critical point of pure water. The critical point locus for water + *n*-alkane mixtures is interrupted and shows gas−gas equilibria of the second kind. De Loos et al.[45] have made measurements of PTx properties for fluid water + *n*-alkane systems on the phase boundary for seven compositions in the temperature range from 600 to 675 K and at pressures from 15 to 170 MPa. De Loos et al.[46] and Yiling et al.[47] have measured the phase equilibria (PTx) and critical properties (P_C, T_C, x_C) in water + *n*-hexane mixtures in the temperature range from 610 to 675 K and at pressures from 15 to 140 MPa. The critical locus between the pure water and pure *n*-hexane critical points (see Figure 1) is not continuous. The lower branch of the critical curve (see Figure 1b) starts from the critical point of *n*-hexane (CP2) and terminates at the upper critical end point (UCEP). The upper branch of the critical curve (see Figure 1a) originates at the pure water critical point (CP1) and extends toward very high pressures and has a minimum with respect to temperature at the point where the two-phase region separates into two parts (G-G and L-G critical loci). The values of the critical temperature T_{Cm}, critical pressure P_{Cm}, and concentration x_{cm} at the temperature minimum of the critical curve for the water + *n*-hexane system are[69] T_{Cm} = 627.8 K, P_{Cm} = 31.0 MPa, and x_{cm} = 0.063 mol fraction of *n*-hexane.

Abdulagatov et al.[49−52] reported $PVTx$ data and virial coefficients for water + *n*-hexane mixtures along six isotherms, (523.15, 573.15, 623.15, 643.15, 647.05, and 648.15) K, for 32 compositions between 0.0268 and 0.9399 mol fraction of *n*-hexane. Pressures ranged from 2 to 40 MPa and densities from 9 to 496 kg·m^{-3}. More precise experimental $PVTx$ data for infinitely dilute water + *n*-hexane mixtures near the solvent's (pure water) critical point were reported recently by Abdulagatov et al.[53] Measurements were carried out for four compositions

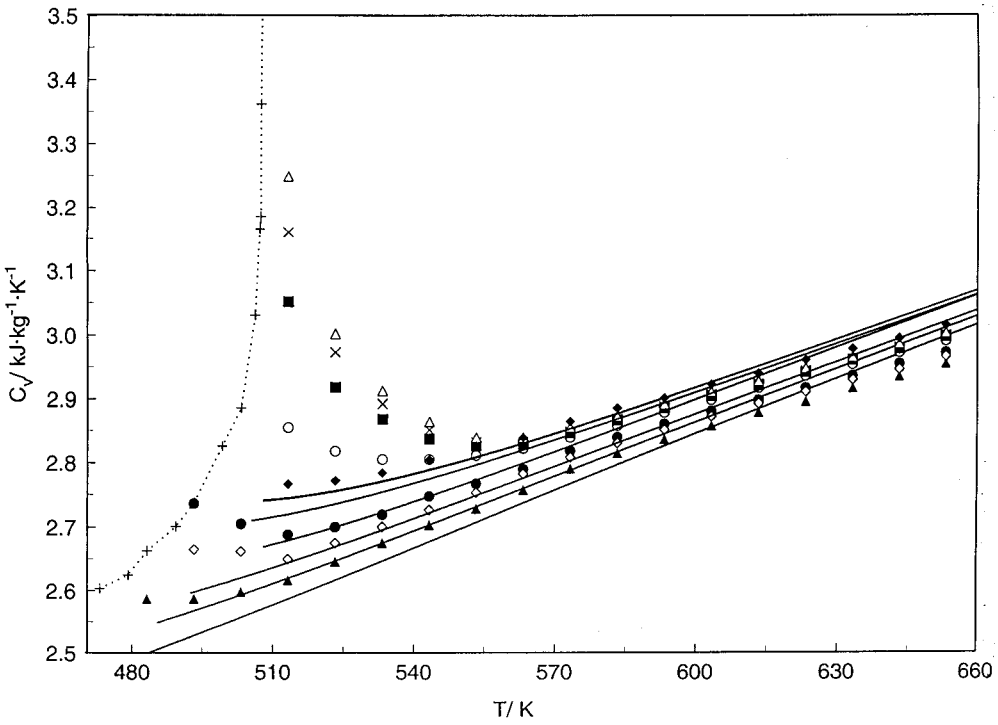

Figure 3. Comparison between measured (Amirkhanov et al.[72]) and calculated (Span[74]) values of C_V for *n*-hexane; the solid lines are calculated from Span's EOS:[74] ▲, 62.50 kg·m^{-3}; ◇, 83.33 kg·m^{-3}; ●, 100.00 kg·m^{-3}; ○, 165.84 kg·m^{-3}; ■, 210.08 kg·m^{-3}; ×, 222.22 kg·m^{-3}; △, 234.08 kg·m^{-3}; ◆, 322.89 kg·m^{-3}; +, values of C_V on coexistence curve.

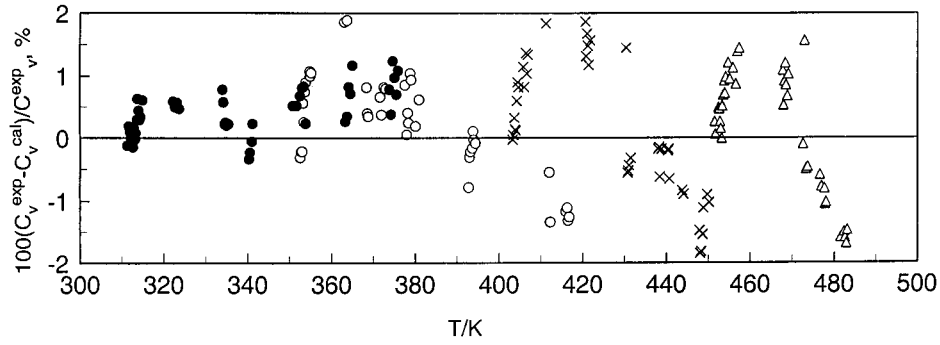

Figure 4. Percentage heat capacity C_V deviations, $\delta C_V = 100[(C_V^{exptl} - C_V^{calcd})/C_V^{exptl}]$, of the experimental heat capacities (Amirkhanov et al.[63]) from the values calculated with the the IAPWS-95 formulation:[73] ●, 992.16 kg·m^{-3}; ○, 971.82 kg·m^{-3}; ×, 933.97 kg·m^{-3}; △, 886.92 kg·m^{-3}.

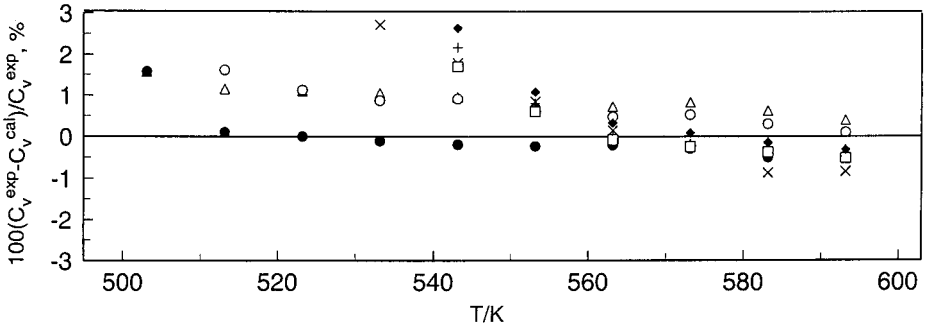

Figure 5. Percentage heat capacity C_V deviations, $\delta C_V = 100[(C_V^{exptl} - C_V^{calcd})/C_V^{exptl}]$, of the experimental heat capacities (Amirkhanov et al.[72]) from the values calculated with the Span[74] EOS: △, 62.50 kg·m^{-3}; ●, 83.33 kg·m^{-3}; ○, 100.00 kg·m^{-3}; ×, 165.84 kg·m^{-3}; □, 210.08 kg·m^{-3}; +, 222.22 kg·m^{-3}; ◇, 234.08 kg·m^{-3}.

(0.0021, 0.0050, 0.0085, and 0.0138 mol fraction of *n*-hexane) along five near-critical and supercritical isotherms, (643.05, 645.05, 647.05, 649.05, and 651.05) K, for pressures from 8 to 35 MPa using a constant-volume piezometer. The uncertainties of these data are as follows: density, 0.2%; pressure, 5 kPa; temperature, 10 mK; and concentration, 0.001 mol fraction. More recently, partial molar volumes at infinite dilution from densimetric measurements were reported for water + *n*-hexane mixtures by Majer et al.[54] at temperatures from 573 to 623 K and at pressures to 30 MPa. Tsonopoulos and Wilson[55] reported three-phase equilibrium pressures for water + *n*-hexane

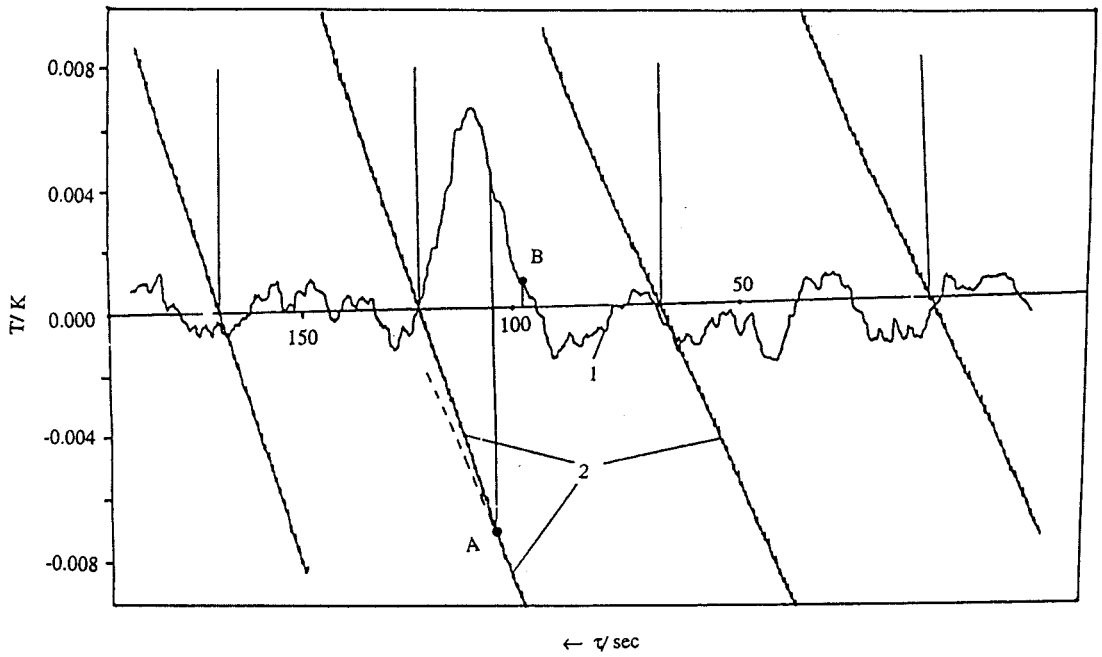

Figure 6. Typical thermogram *(T−τ)* of the sample's temperature variation along fixed density 262.47 kg·m^{-3} and concentration 0.994 mol fraction of C_6H_{14} and record of the adiabatic condition for the water + *n*-hexane mixture: 1, record of the adiabacity condition; 2, thermogram *(T−τ)*; *A*, phase transition point on the thermogram; *B*, phase transition point on the adiabatic condition curve.

mixture at temperatures from 313 to 422 K. The temperature dependence of three-phase equilibrium pressures were represented by a two-term equation[55]

$$\ln P = 9.8127 - 4047.7\ T^{-1} \qquad (1)$$

The excess enthalpy H^E of water−*n*-hexane vapor has been measured by Wormald et al.,[56−58] using a flow mixing calorimeter in the temperature range from 373 to 698 K at a pressure of 12 MPa for compositions from 0.369 to 0.611 mol fraction of *n*-hexane. The cross-term second virial coefficients B_{12} and cross-term isothermal Joule−Thomson coefficient Φ_{12} for water−*n*-hexane have been derived from the excess enthalpies. A high-pressure flow calorimeter for the measurements of H^E at temperatures up to 700 K was constructed and used to measure H^E for water + *n*-hexane.[56] High-pressure H^E measurements have been used to calculate excess volumes V^E and compressibility factors *Z* for water + *n*-hexane mixtures.[56] An alternative to enthalpy measurements (H^E) is accurate C_VVTx measurements, which can be used for testing the agreement of the two different kinds of measurements.

Neichel and Franck[59] calculated the critical curves for water + *n*-hexane mixtures at temperatures up to 670 K and at pressures up to 200 MPa using a perturbation type equation of state (EOS) with a repulsion term and an attraction term with a square-well potential for intermolecular interaction. The three adjustable parameters of the model (k_σ, k_ϵ, and w_{ij}) have been calculated using (P_C, T_C, and x_C) critical locus data. A modified Soave−Redlich−Kwong equation of state with an exponent-type mixing rule for the energy parameter and a conventional mixing rule for the size parameter is applied to correlate the phase equilibria for binary mixtures of water + *n*-hexane at high temperatures and pressures by Haruki et al.[60,61] The three-phase (L-L-G) equilibria for water + hydrocarbon mixtures of interest in the thermal recovery of crude oil via steam distillation were measured by Eubank et al.[62] A Peng−Robinson equation of state model was developed to predict these data. The improved equations for prediction of the binary interaction constants k_{ij} were also presented. The *P−T* phase diagram for the water + *n*-hexane mixture from the literature data is shown in Figure 1.

Experimental Section

Measurements of the isochoric heat capacity of aqueous *n*-hexane mixtures were made in a high-temperature, high-pressure nearly constant integrated adiabatic calorimeter, of a design pioneered by Amirkhanov et al.[63] The construction, method of measurements, and detailed analysis of all sources of uncertainty of the measurements have been described in our previous papers,[39−44,64−68] and they will be only briefly reviewed here. For the present measurements we used a calorimeter with a volume of $V_0 = 100.085 \pm 0.0002$ cm^3 at room temperature (25 °C) and atmospheric pressure. The temperature was measured with a miniature standard resistance thermometer type PRT-10 mounted in a tube inside the calorimetric sphere with an uncertainty of 10 mK. The pressure was measured with dead-weight pressure gauges MP-60 and MP-600 with uncertainties of 0.05%. The heating time was fixed by means of a frequency meter (F5041) with an uncertainty of 0.01 s.

The volume $V(P,T)$ of the empty calorimeter at given *T* and *P* is necessary to know for the purpose of calculating densities of measuring fluid as the ratio of the mass of the sample *m* to the working volume $V(P,T)$, $\rho = m/V(P,T)$. The volume of the empty calorimeter at *T* and *P* was calculated from

$$V(P,T) = V_0 + \Delta V_T + \Delta V_P \qquad (2)$$

with

$$\Delta V_T = 3\alpha\,(t - 25)V_0 \text{ and } \Delta V_P = \beta(P - 0.1)V_0$$

where $\alpha = (1.66-1.75) \times 10^{-5}$ K^{-1} (at temperatures from 373 to 673 K) is the thermal expansion coefficient of the calorimeter vessel material (1X18H9T) and *t* is the temperature in °C. The pressure expansion $V(P)$ was determined by calculation using the Love formula ($\beta = 2.2978$

Table 1. Experimental Values of the Heat Capacities C_{VX} along Isochores in Aqueous *n*-Hexane Mixtures for Various Concentrations

$x = 0.9940$ mol fraction of C_6H_{14}, $\rho = 259.34$ kg·m^{-3}

T (K)	C_{VX} (kJ·K^{-1}·kg^{-1})	T (K)	C_{VX} (kJ·K^{-1}·kg^{-1})
497.15	3.89	499.62	4.06
497.34	3.88	500.00	4.16
497.53	3.87	500.19	4.19
497.72	3.91	500.38	4.27
497.91	3.92	500.57	4.47
498.29	3.94	500.76	4.68
498.48	3.92	501.14	3.11
498.67	3.99	501.33	3.02
499.05	4.01	501.51	3.01
499.24	4.05	501.91	3.00
499.43	4.08		

$x = 0.9892$ mol fraction of C_6H_{14}, $\rho = 262.47$ kg·m^{-3}

T (K)	C_{VX} (kJ·K^{-1}·kg^{-1})	T (K)	C_{VX} (kJ·K^{-1}·kg^{-1})
496.00	4.38	497.13	4.62
496.19	4.39	497.32	4.93
496.38	4.46	497.51	3.16
496.57	4.45	497.70	3.05
496.76	4.50	497.89	3.06
496.75	4.55	498.08	2.99
496.94	4.58	498.27	2.95

$x = 0.9940$ mol fraction of C_6H_{14}, $\rho = 262.47$ kg·m^{-3}

T (K)	C_{VX} (kJ·K^{-1}·kg^{-1})
425.57	3.44
425.97	3.45
434.40	3.48
434.60	3.49
435.00	3.50
442.68	3.56
443.08	3.56
454.53	3.84
454.73	3.88
454.93	3.95
455.13	4.15
455.33	3.82
455.53	3.73
455.73	3.60
455.93	3.57
456.13	3.25
456.33	3.14
456.73	3.08
456.93	3.09
463.80	3.12
464.20	3.14

$x = 0.9892$ mol fraction of C_6H_{14}, $\rho = 262.47$ kg·m^{-3}

T (K)	C_{VX} (kJ·K^{-1}·kg^{-1})
480.24	4.70
480.53	4.72
480.72	4.75
480.91	4.78
481.10	4.76
481.29	4.78
481.48	4.76
481.67	4.77
481.86	4.76
482.05	4.73
482.24	4.72
482.43	4.70
482.62	4.51
482.81	4.35
483.00	4.17
483.19	4.06
483.38	3.91
483.57	3.90
483.76	3.89

$x = 0.9858$ mol fraction of C_6H_{14}, $\rho = 262.12 \cdot 10^{-3}$ kg·m^{-3}

T (K)	C_{VX} (kJ·K^{-1}·kg^{-1})
491.25	5.47
491.44	5.50
491.63	5.51
491.82	5.57
492.01	5.56
492.21	5.63
492.40	5.59
492.59	5.64
492.78	5.69
492.97	5.78
493.16	5.80
493.54	5.76
493.73	5.56
493.92	5.23
494.11	4.32
494.31	4.24
494.50	4.23

$x = 0.9775$ mol fraction of C_6H_{14}, $\rho = 265.89$ kg·m^{-3}

T (K)	C_{VX} (kJ·K^{-1}·kg^{-1})	T (K)	C_{VX} (kJ·K^{-1}·kg^{-1})
503.55	4.61	515.22	4.82
503.74	4.63	515.41	4.81
503.93	4.62	515.79	4.81
504.12	4.62	515.98	4.73
507.33	4.60	516.36	4.41
507.52	4.59	516.55	4.09
507.71	4.60	517.50	3.69
512.56	4.75	517.69	3.54
512.75	4.78	517.88	3.45
512.94	4.80	518.07	3.38
513.12	4.79		

$x = 0.9349$ mol fraction of C_6H_{14}, $\rho = 269.54$ kg·m^{-3}

T (K)	C_{VX} (kJ·K^{-1}·kg^{-1})	T (K)	C_{VX} (kJ·K^{-1}·kg^{-1})
563.21	5.71	568.61	6.77
563.39	5.75	568.97	6.76
563.57	5.81	569.15	6.80
563.75	5.84	569.51	6.79
565.19	6.18	569.87	6.82
565.37	6.20	570.05	6.82
565.55	6.28	570.23	6.81
565.73	6.31	570.59	6.76
567.89	6.71	570.95	6.65
568.07	6.73	571.31	6.50
568.25	6.72		

$x = 0.9775$ mol fraction of C_6H_{14}, $\rho = 265.89$ kg·m^{-3}

T (K)	C_{VX} (kJ·K^{-1}·kg^{-1})
518.45	3.33
518.64	3.29
520.16	3.08
520.35	3.06
520.54	3.05
520.73	3.05
523.01	2.96
523.20	2.96
523.39	2.95
523.58	2.95

$x = 0.9349$ mol fraction of C_6H_{14}, $\rho = 269.54$ kg·m^{-3}

T (K)	C_{VX} (kJ·K^{-1}·kg^{-1})	T (K)	C_{VX} (kJ·K^{-1}·kg^{-1})	T (K)	C_{VX} (kJ·K^{-1}·kg^{-1})
372.62	3.18	494.21	7.15	563.21	5.71
372.89	3.20	494.40	7.55	563.75	5.84
373.11	3.19	494.59	7.08	565.19	6.18
373.33	3.21	494.78	5.84	565.73	6.31
423.90	3.81	494.97	5.16	567.89	6.71
424.31	3.83	495.54	4.81	568.97	6.76
424.72	3.84	495.73	4.75	569.15	6.80
478.89	5.07	495.92	4.68	570.05	6.82
479.33	5.05	496.11	4.69	570.95	6.65
479.52	5.08	496.30	4.66	571.31	6.50
479.71	5.12	496.49	4.68	571.49	6.44
489.73	5.77	496.68	4.65	571.67	6.32
489.92	5.83	510.74	4.72	571.85	6.14
490.68	6.13	532.47	4.98	572.03	5.72
490.87	6.14	532.65	4.99	572.21	5.40
491.06	6.17	532.83	4.96	572.39	4.89
492.69	6.40	533.02	4.99	572.57	4.06
492.88	6.34	551.36	5.65	572.75	3.45
493.07	6.38	551.54	5.69	572.93	3.11
493.26	6.49	551.72	5.66	574.01	2.98
493.45	6.67	551.90	5.67	574.19	2.99
493.64	6.74	556.94	5.88	574.37	2.98
493.83	6.81	557.12	5.87	574.55	2.97
494.02	7.03	557.30	5.90		

Table 1 (Continued)

$x = 0.9775$ mol fraction of C_6H_{14} $\rho = 262.88$ kg·m^{-3}		$x = 0.9349$ mol fraction of C_6H_{14} $\rho = 286.53$ kg·m^{-3}		$x = 0.7965$ mol fraction of C_6H_{14} $\rho = 284.09$ kg·m^{-3}		$x = 0.6146$ mol fraction of C_6H_{14} $\rho = 312.50$ kg·m^{-3}	
T (K)	C_{VX} (kJ·K^{-1}·kg^{-1})	T (K)	C_{VX} (kJ·K^{-1}·kg^{-1})	T (K)	C_{VX} (kJ·K^{-1}·kg^{-1})	T (K)	C_{VX} (kJ·K^{-1}·kg^{-1})
463.20	4.73	491.18	6.14	491.83	5.90	482.10	4.78
463.60	4.73	491.37	6.19	492.02	6.04	482.29	4.77
468.05	4.82	491.56	6.14	492.21	5.90	482.49	4.80
468.24	4.84	491.75	6.23	492.40	5.82	482.68	4.79
477.76	5.15	493.84	6.68	492.59	5.87	483.07	4.20
477.95	5.19	494.03	6.89	492.78	4.91	483.26	4.12
489.34	6.04	494.22	6.95	492.97	4.45	483.45	4.05
489.53	6.06	494.41	7.24	493.16	4.39	483.64	4.03
493.65	6.77	494.60	7.57	493.35	4.40	483.84	3.96
493.84	6.80	494.79	5.92	493.54	4.38	484.05	4.00
494.03	6.93	495.17	4.89	493.73	4.35		
494.22	7.17	495.36	4.67	493.92	4.37		
494.41	7.41	495.54	4.62	494.11	4.35		
494.60	7.79	495.73	4.55	494.30	4.36		
494.78	5.26			494.49	4.37		
495.17	5.02						
496.59	4.79						
503.41	4.61						
503.60	4.63						
503.98	4.60						

$\times 10^{-6}$ bar^{-1}) for spherical vessel[69,70] and determined experimentally using the method developed by Bochkov.[70] The uncertainty in volume estimate at any T and P in our experiment is ~0.05−0.09%. The mass of the sample was measured using the weighing method with an uncertainty of 0.05 mg. Therefore, the uncertainty in density measurements $\rho = m/V(P,T)$ is ~0.06−0.10%.

The heat capacity of the empty calorimeter C_0 was determined experimentally using a reference substance (helium-4) with well-known isobaric heat capacities,[71] in the temperature range up to 1000 K at pressures up to 20 MPa. The results of these measurements for C_0 can be described by the equation

$$C_0/(\mathrm{J\cdot K^{-1}}) = 81.2 + 0.069(t/^\circ\mathrm{C}) \qquad (3)$$

This equation reproduced experimental values of C_0 within ±0.9%.

The heat capacity was obtained from the measured quantities m, ΔQ, ΔT, and C_0. The uncertainties in these measured quantities are $\delta(\Delta Q) = 0.02\%$, $\delta(\Delta T) = 0.1\%$ for $\Delta T = (0.5-1.0)$ K and $\delta(\Delta T) = 0.5\%$ for $\Delta T = (0.02-0.05)$ K, $\delta(C_0) = 0.3\%$ at low temperatures and $\delta(C_0) = 1.0\%$ at high temperatures, and $\delta(m) = 0.02\%$. On the basis of the detailed analysis of all measurement [$\delta(\Delta Q)$, $\delta(\Delta T)$, $\delta(C_0)$, and $\delta(m)$] and nonmeasurement sources of uncertainties likely to affect the determination of C_V with the present system, the combined standard uncertainty of measuring the heat capacity with allowance for the propagation of uncertainty related to the nonisochoric conditions of the process was 0.5−1.0% in the liquid phase, 1.0−1.5% in the critical region, and 1.0−3.5% in the vapor phase.

The previous measurements of pure components (water[63] and *n*-hexane[72]) using this calorimeter confirmed the reliability of the present calorimetric apparatus. The agreement between experimental C_V data for pure water[63] and the IAPWS-95 formulation[73] and between C_V data for pure *n*-hexane[72] and the Span[74] multiparametric fundamental equation of state are within ±2% and ±3%, respectively. Figures 2 a−d and 3 show the comparison between measured and calculated values of C_V for water and *n*-hexane. The deviation plots are shown in Figures 4 and 5. The deviation statistics are as follows: for water, $N = 175$, maximum deviation = −2.39, bias = 0.29, standard deviation = 0.92, standard error = 0.07, and AAD = 0.75%; for *n*-hexane, $N = 56$, maximum deviation = 3.39, bias = 0.62, standard deviation = 0.98, standard error = 0.13, and AAD = 0.56%. Excellent agreement between values of C_V measured for pure water[63] using this calorimeter and values measured by Magee et al.[75] and values calculated from IAPWS-95[73] are observed. Good agreement between C_V measurements for *n*-hexane and values calculated from the Span[74] EOS are observed in the temperature range from 500 to 660 K for densities far from the critical and phase transition points.

This method enables one to accurately determine the phase transition temperature T_S of the system from the three-phase (L-L-G) to the two-phase (L-L, L-G) state and from the two-phase (L-L, L-G) to a single-phase (L or G) state (i.e., to determine T_S and ρ_S data corresponding to the phase transition curves for each fixed composition), the jump in the heat capacity ΔC_V, and reliable C_V data in the single-phase (liquid and vapor), two-phase (L-L, L-G), and three-phase (L-L-G) regions. The techniques of determining parameters T_S and ρ_S at the phase transition curves and measuring heat capacity C_V at this curve are similar to the method of quasi-static thermograms.[76,77] Measurements of the temperatures T_S and densities ρ_S corresponding to the phase transition curves using the method of quasi-static thermograms are described in detail by Polikhronidi et al.[64−68] In the C_V experiments the state of the calorimetric system is controlled with two independent sensors, namely, (1) a resistance thermometer (PRT-10) (thermograms, $T-\tau$ plots, see Figure 6, curve 2) and (2) a layer of cuprous oxide serving as an adiabatic shield (see Figure 6, curve 1). Figure 6 show some typical thermograms [($T-\tau$) plots] and a record of the adiabatic condition for the water + *n*-hexane mixture along isochore 262.47 kg·m^{-3} and concentration of $x = 0.994$ mol fraction of C_6H_{14}. Synchronous recording readings of the resistance thermometer (Figure 6, curve 2) and of the sensor of adiabaticity (Figure 6, curve 1) allow one to follow the state of the sample upon approaching the phase transition points. On intersecting the phase transition (L-L-G, L-L, and L-G) curves, the heat capacity is known to change discontinuously, leading to a sharp change in the thermogram slope ($dT/d\tau$). This process can be very clearly read by recording thermograms ($T-\tau$ plots) and from the adiabatic sensor (see Figure 6, points A and B). The high sensitivity of cuprous oxide makes it possible to fix immediately the temperature changes on a strip-chart recorder. Temperature changes are recorded on a thermogram tape of a pen-recorder as a spike produced by the sensor of adiabaticity and as a break (change of the thermogram slope). The coincidence in time of the positions

of the spike in the adiabaticity-sensor signal and of the break in the thermogram of the sample (positions of points A and B) indicates that the processes occurring in the system are quasi-static. Indeed, the cuprous oxide responds to a change in the thermodynamic state of the sample at the internal surface of the calorimeter, whereas the resistance thermometer records temperature changes in the center of the calorimeter. The presence of temperature gradients in the volume of the sample had to shift the positions of the spike and the break in the thermogram on the tape of the pen-recorder. However, with temperature changes occurring at rates of 5×10^{-5} to 10^{-4} K·s^{-1}, the shift is not more than 10^{-4} K. At $dT/d\tau > 0$, the thermogram experiences a break when intersecting the phase transition curve because of a jump in the heat capacity ΔC_V. At this moment, the temperature difference set at the layer of cuprous oxide and ensuring the adiabaticity of the calorimetric system becomes disturbed for a short period (1−2 s, see Figure 6, point B). In the process of measurement, the adiabaticity of the system was disturbed, which is fixed by the pen-recorder as small undamped oscillations with an amplitude of 5×10^{-5} K. At the moment of the transition, the disturbed adiabaticity becomes more pronounced and represents decaying oscillations with an initial amplitude of 2×10^{-3} K. The uncertainty in phase transition temperature T_S measurements in this method is ~0.02 K. The rate of temperature change $dT/d\tau$, determined by the power supplied to the internal heater, varied from 2.7×10^{-4} to 5×10^{-4} K·s^{-1}, depending on the region where the investigation was carried out.

High-purity samples of H_2O and *n*-hexane were obtained to prepare the mixtures. The H_2O sample was twice-distilled and has an electrical conductivity of 10^{-4} Ω^{-1}·m^{-1}. For the *n*-hexane sample, the commercial supplier claimed a minimum liquid purity of 0.9986 mass fraction with 0.0014 mass fraction of *n*-hexane isomers. Each component was degassed twice.

Results

The isochoric heat capacity data for water + *n*-hexane mixtures were obtained for seven compositions: (0.6146, 0.7965, 0.9349, 0.9775, 0.9858, 0.9892, and 0.9940) mol fraction of *n*-hexane along seven near-critical isochores between 259.34 and 312.50 kg·m^{-3} in the temperature range from (463 to 522) K at pressures up to 6 MPa. The data are listed in Table 1. The typical temperature dependence of the isochoric heat capacity along various isochores and compositions is shown in Figure 7. Two peaks or jumps in the isochoric heat capacity are often found. The discontinuity in C_V behavior at the intersection of the phase boundary curve is connected with liquid−liquid and liquid−gas-phase transitions occurring in a binary water + *n*-hexane mixture heated in a closed volume. Heating the three-phase (L-L-G) water + *n*-hexane mixture can lead to three different sequences of phase transitions, depending on the fill coefficient (ratio of the volume of the mixture to the volume of the calorimeter at ambient temperature) or the average fill density (ratio of the mass of mixture to the volume of the calorimeter at ambient temperature) and the *n*-hexane concentration in the initial mixture.

(1) At highest average densities and high concentration of *n*-hexane, the liquid phase expands on heating and fills the entire vessel, whereas the vapor phase disappears. A transition from three phases (L-L-G) to two phases (L-L) (L-L-G ⇔ L-L) occurs, with a drop in heat capacity. A transition from two-phase (L-L) equilibria to one-phase (L) (L-L ⇔ L) takes place at further isochoric heating of the mixture.

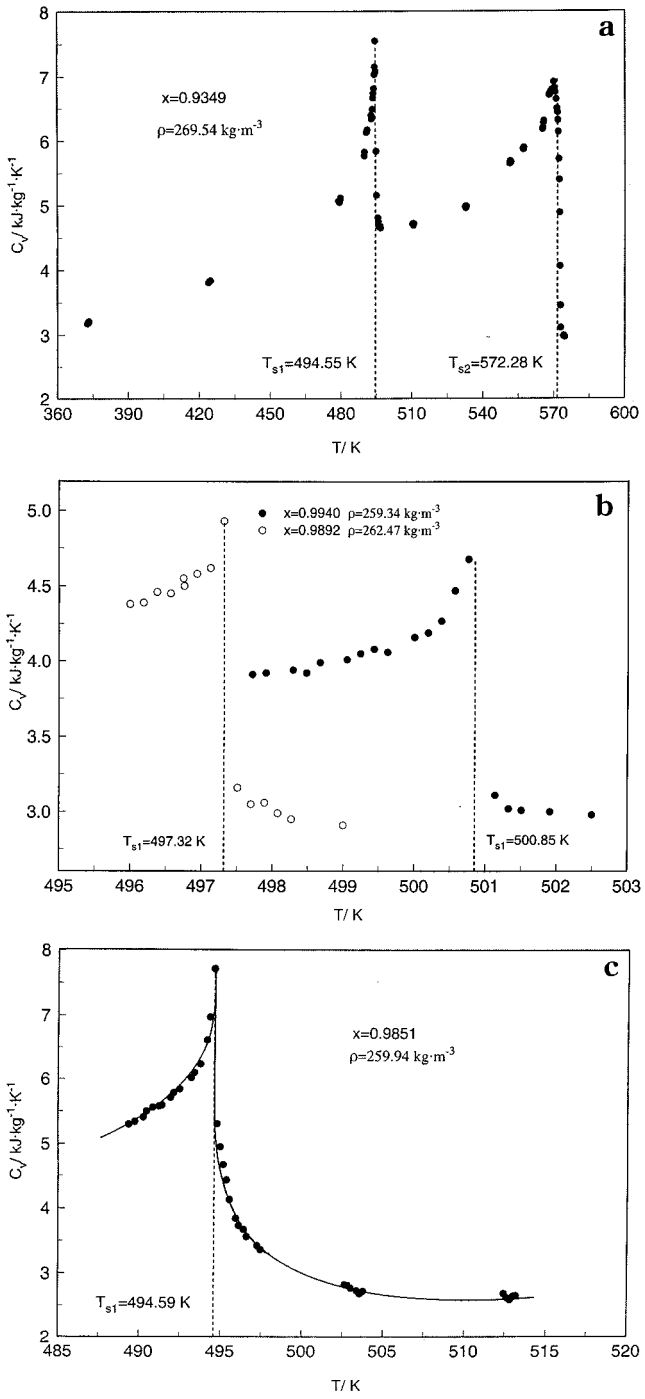

Figure 7. Typical isochoric heat capacity behavior as a function of temperature along various isochores and compositions.

(2) At the highest average densities and low concentration of *n*-hexane, before the thermal expansion causes the liquids to fill the entire volume, the initially immiscible liquid water + *n*-hexane mixture becomes miscible due to the positive temperature coefficient of solubility typical for water + *n*-alkane mixtures. In this case, the first phase transition is the miscibility of *n*-hexane in water in equilibrium with its vapor (L-L-G ⇔ L-G), with a decrease in heat capacity as the number of phases decreases. On further heating of the two-phase (L-G) mixture, the expanding liquid fills the entire cell, whereas the vapor phase disappears. A transition from two-phase (L-G) to one-phase (L) (L−G ⇔ L), takes place, with a decrease in heat capacity.

Table 2. Compositions (x), First (T_{S1}) and Second (T_{S2}) Peaks or Jumps in C_{VX} Temperatures, and Averaged Densities (ρ) on the Three- and Two-Phase Transition Points

x (mol fraction of C_6H_{14})	T_{S1} (K)	T_{S2} (K)	ρ (kg·m^{-3})
0.9940	456.15	500.85	245.46
0.9892	482.45	497.35	262.47
0.9858	492.78	495.15	257.60
0.9851	494.69	494.69	259.94
0.9816	494.69	505.65	264.20
0.9775	494.65	515.23	262.88
0.9349	494.55	572.28	286.53
0.8271	492.97	608.11	262.47
0.7965	492.70	615.22	284.09
0.6146	484.61	628.77	312.89
0.3470	445.15	631.85	317.46
0.1289	395.75	644.20	303.03

(3) At the lowest average densities, heating increases the vapor density, resulting in the disappearance of the liquid phases. A transition takes place from three-phase (L-L-G) to two-phase equilibria (L-G) (L-L-G ⇔ L-G), again with a drop in the heat capacity. A transition from two-phase (L-G) equilibria to one-phase (G) (L-G ⇔ G) takes place, at further isochoric heating of the mixture.

Cases 2 and 3 have been encountered in our experimental data (see Figure 7). The first peak marks the disappearance of a liquid phase, and the second peak marks the disappearance of the liquid or vapor phase. The values of measured temperature at the first and second peaks are presented in Table 2 together with values of filled density and initial filled composition. Case 1 has never been found in our experiments. As one can see from Table 2 the difference between the first and second peaks $\Delta T_S = T_{S2} - T_{S1}$ depends on initial filled densities and compositions. For example, for the isochore 259.94 kg·m^{-3} and composition $x = 0.9851$ mol fraction of *n*-hexane we found only one peak in the temperature dependence of C_V (see Figure 7c) where both jumps take place at the same temperature, $\Delta T_S = 0$. This isochore intersects the phase transition temperature at the UCEP, where the three-phase curve L-L-G intersects the L = G critical curve. Therefore, Figure 7c represents the temperature-dependent behavior of C_{VX} for the water + *n*-hexane mixture near the UCEP. For the first time we have studied the temperature dependence of C_{VX} near the UCEP.

In Figure 8, the density of the fluid along the three-phase curve is plotted. The measured densities on the three-phase curve define a smooth curve, with a temperature maximum at 495.82 K. This maximum corresponds to the UCEP, where the densities of the liquid and vapor mixtures in the three-phase equilibrium become identical or the same as the intersection of the critical curve (L = G) and the three-phase solubility curve (L-L-G) (see Figure 1b). The UCEP is located ~8 K below the *n*-hexane critical point[78] (507.85 K). The available literature data on the UCEP parameters for the water + *n*-hexane mixture are given in Table 3. Our results for the UCEP temperature $T_{UCEP} = 495.82$ K and UCEP pressure $P_{UCEP} = 5.250$ MPa are in good agreement (differences are $\Delta T_{UCEP} = 0.63$ K and $\Delta P_{UCEP} = 0.02$ MPa) with the values reported by other authors.[21,48,55,79,80] However, the maximum deviation between the present UCEP temperature and the data reported by Tsonopoulos and Wilson[55] was 0.88 K and the UCEP pressure differs by 0.045 MPa (Roof[80]). For the first time we reported the values of UCEP density $\rho_{UCEP} = 259.94$ kg·m^{-3} for the water + *n*-hexane mixture. The measured values of pressure on the three-phase curve are presented in Table 4 and Figure 1b. The agreement between the present measured values of three-phase pressure and values calculated with eq 1 is within ±0.75%. Figure 9 shows a comparison of experimental values of densities on the two-phase boundary for the water + *n*-hexane mixture ($x = 0.61$ mol fraction of *n*-hexane) derived from present calorimetric (C_{VX}) measurements and from thermal ($PVTx$) measurements by Yiling et al.[47] As Figure 9 shows, the agreement is satisfactory.

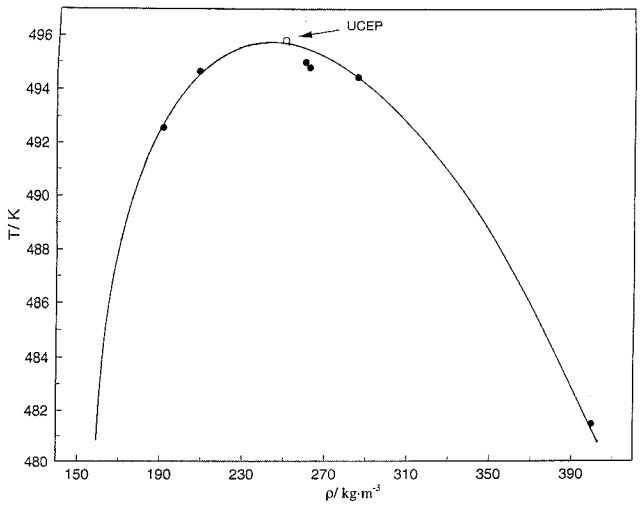

Figure 8. Temperature dependence of the density on the three-phase curve up to the critical end point for the water + *n*-hexane mixture; the maximum temperature $T_{UCEP} = 495.82$ K corresponds to the UCEP, where the densities of liquid and vapor mixture ($\rho_{UCEP} = 250.94$ kg·m^{-3}) in the three-phase equilibrium become identical.

Table 3. Values of UCEP Temperature, Pressure, and Density for Water + *n*-Hexane Mixtures

T_{UCEP} (K)	P_{UCEP} (MPa)	ρ_{UCEP} (kg·m^{-3})	ref
496.7	5.270		Tsonopoulos and Wilson[55]
495.15	5.275		Rebert and Hayworth[21]
495.21	5.274		Scheffer[79]
496.48	5.295		Roof[80]
496.40	5.282		Brunner[48]
495.82	5.250	259.94	this work

Table 4. Three-Phase Equilibrium Pressures for Water + *n*-Hexane Mixtures

T_S (K)	P_S (MPa)	T_S (K)	P_S (MPa)	T_S (K)	P_S (MPa)
395.75	0.67	481.45	4.10	494. 65	5.16
455.25	2.49	492.56	4.95	494.50	5.20
456.15	2.55	492.97	4.95	494.69	5.22
477.00	3.76	494.45	5.02	494.82	5.25

Table 5. Average Density Data for Water + *n*-Hexane Mixture (x = 75 wt % H_2O) on the Three-Phase Equilibrium Curve

T_S (K)	ρ_S (kg·m^{-3})	T_S (K)	ρ_S (kg·m^{-3})
492.46	401.3	477.28	263.1
488.83	351.0	468.52	219.8
484.61	312.9	477.00	260.4
482.88	297.6		

Figure 10 shows the critical temperature of water + *n*-hexane mixtures as a function concentration. The critical curve for the water + *n*-hexane mixture was expressed as

$$T_C(x) = T_C(H_2O)(1 - x) + T_C(C_6H_{14})x + (1 - x)\sum_{i=1} T_i x^i \quad (4)$$

where $T_C(H_2O) = 647.096$ K is the critical temperature of pure water[81] and $T_C(C_6H_{14}) = 507.85$ K is the critical

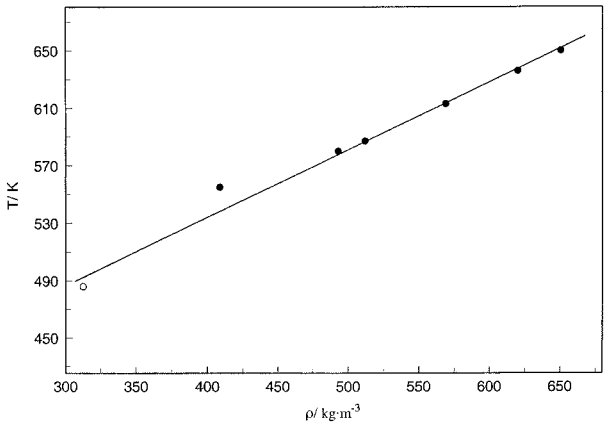

Figure 9. Experimental values of densities for constant molar fractions of *n*-hexane ($x = 0.610$) along two-phase boundary as a function of temperature for the water + *n*-hexane mixture: ●, Yiling et al.;[47] ○, this work; solid curve is a guide to the eye.

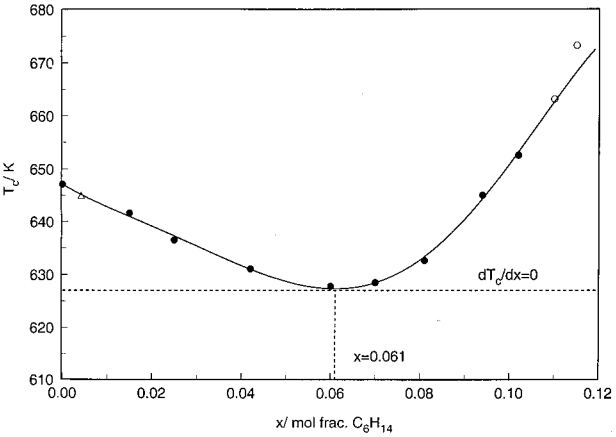

Figure 10. Critical temperature for the water + *n*-hexane mixture as a function of concentration; the solid line is calculated from eq 4: ●, De Loos et al.;[46] ○, Yiling et al.;[47] △, Rebert and Hayworth.[21]

temperature of pure *n*-hexane.[78] The values of constants T_i derived from experimental data[21,46,47] are $T_1 = -3.778124 \times 10^2$, $T_2 = 1.17860546 \times 10^4$, $T_3 = 4.132518596 \times 10^5$, $T_4 = 5.772977022 \times 10^6$, $T_5 = -2.2442830641 \times 10^7$. According to the theory of critical phenomena for binary mixtures,[82−86] the asymptotic behavior of isochoric heat capacity C_{VX} along the critical isochores $\rho = \rho_C(x)$ at fixed concentration x is determined by the characteristic temperature

$$\tau_\alpha(x) \cong \left[A_0 x(1-x)\left(\frac{1}{T_C(x)}\frac{dT_C}{dx}\right)^2\right]^{1/\alpha} \qquad (5)$$

where $A_0 = 7.342$ is the nonuniversal critical amplitude for pure water[87] and $\alpha = 0.112$ is the universal critical exponent for isochoric heat capacity.[88]

In the temperature range $\tau_\alpha(x) \ll \tau(x) \ll 1$ the isochoric heat capacity at constant x behaves as a scaling power law for pure fluids:

$$\frac{C_{VX}}{R} \approx A_0 \tau(x)^{-\alpha} + \text{constant} \qquad (6)$$

However, at temperatures asymptotically close to the critical point

$$\tau(x) \ll \tau_\alpha(x) \qquad (7)$$

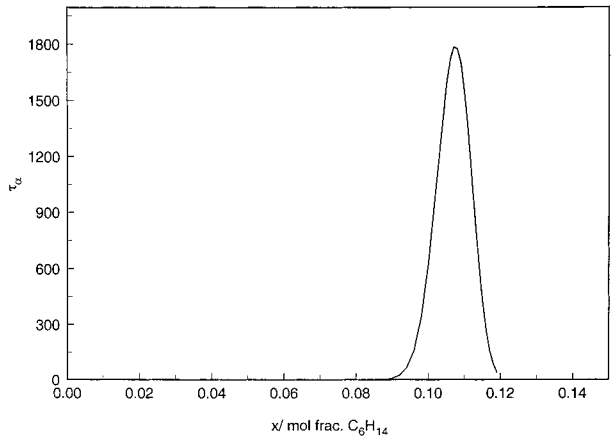

Figure 11. Characteristic temperature $\tau_\alpha(x)$ as a function of the concentration of *n*-hexane.

the renormalization of the critical exponent $\alpha \rightarrow -\alpha/(1-\alpha)$ takes place. Therefore, C_{VX} on the critical isochore behaves as

$$C_{VX} \approx \text{constant} - \tau(x)^{\alpha/(1-\alpha)} \qquad (8)$$

At a concentration of $x = 0.06103$ mol fraction of C_6H_{14}, the derivative $dT_C/dx = 0$ is equal to zero; therefore, according to eq 5, $\tau_\alpha(x) \rightarrow 0$ and in the temperature range $0 < \tau(x) < 1$ the isochoric heat capacity of the water + *n*-hexane mixture behaves as for pure fluids. At concentrations $x > 0.084$ mol fraction of C_6H_{14}, the parameter $\tau_\alpha(x) > 10^{-1}$ is not small (see Figure 11); therefore, at $\tau(x) < 10^{-1}$ the renormalization of the critical behavior of C_{VX} is observed. For compositions between 0 and 0.084 mol fraction of C_6H_{14}, the values of $\tau_\alpha(x)$ are almost zero; therefore, C_{VX} along the critical isochores corresponding to these compositions behaves as for pure fluids. Unfortunately, in the present work we measured C_{VX} for the water + *n*-hexane mixture for compositions out of the range where the renormalization of the critical behavior of C_{VX} takes place. Therefore, measurements in the concentration range from 0.084 to 0.12 mol fraction of *n*-hexane (see Figure 11) are needed to experimentally test the renormalization of the critical behavior of C_{VX} for the water + *n*-hexane mixture.

Crossover equations of state for water + toluene mixtures developed by Kiselev et al.[89] have also predicted the renormalization of the isochoric heat capacity critical exponent $\alpha \rightarrow -\alpha/(1-\alpha)$ at concentrations $x > 0.08$ mol fraction of toluene and at temperatures $\tau(x) \ll 10^{-1}$. At concentrations $x < 0.08$ mol fraction of toluene, the value of the parameter $\tau_\alpha(x)$ is small [$\tau_\alpha(x) \ll 10^{-3}$], and in the temperature range $10^{-4} < \tau(x) < 1$ the isochoric heat capacity of water + toluene behaves like C_V for pure fluids. Therefore, this is a general behavior of the dilute water + hydrocarbon mixtures near the critical point of pure water.

Conclusions

New isochoric heat capacity data were presented for aqueous *n*-hexane mixtures for seven compositions, (0.6146, 0.7965, 0.9349, 0.9775, 0.9858, 0.9892, and 0.9940) mol fraction of *n*-hexane, along seven near-critical isochores between 259.34 and 312.5 kg·m^{-3} in the temperature range from (463 to 522) K at pressures up to 6 MPa with an uncertainty of 1.0−1.5%. On isochoric heating, heat capacity data show features such as jumps and spikes, which indicate the occurrence of phase transitions. These transitions are the disappearance of the liquid phase and the

disappearance of a vapor or liquid phase. From the present measurements the upper critical end point temperature, pressure, and density of the water + *n*-hexane system were estimated. The values of three-phase equilibria pressure for water + *n*-hexane mixtures were presented. We demonstrated that isochoric heat capacity measurements are a very sensitive means to determine the location of three-phase (L-L-G) and two-phase (L-L, L-G) boundaries of fluid mixtures near the critical points. At concentrations between 0.084 and 0.120 mol fraction of C_6H_{14} and at temperatures $\tau(x) < 10^{-1}$ the renormalization of the critical behavior of C_{VX} is expected. For compositions between 0 and 0.084 mol fraction of C_6H_{14} and $x > 0.120$ C_{VX} along the critical isochores behaves as for pure fluids. For the first time we reported the values of C_{VX} for the water + *n*-hexane mixture near the UCEP.

Literature Cited

(1) Levelt Sengers, J. M. H.; Morrison, G.; Nielson, G.; Chang, R. F.; Everhart, C. M. Thermodynamic behavior of supercritical fluid mixtures. *Int. J. Thermophys.* **1986**, *7*, 231−243.

(2) Levelt Sengers, J. M. H. Thermodynamics of solutions near the solvent's critical point. In *Supercritical Fluid Technology. Review in Modern Theory and Applications*; Bruno, T. J., Ely, J. F., Eds.; CRC Press: Boca Raton, FL, 1991; pp 1−56.

(3) Levelt Sengers, J. M. H. Solubility near the solvent's critical point. *J. Supercrit. Fluids.* **1991**, *4*, 215−222.

(4) Chang, R. F.; Morrison, G.; Levelt Sengers, J. M. H. The critical dilemma of dilute mixtures. *J. Phys. Chem.* **1984**, *88*, 3389−3391.

(5) Chimowitz, E. H.; Afrane, G. Classical, non-classical critical divergences and partial molar properties from adsorption measurements in near-critical mixtures. *Fluid Phase Equilib.* **1996**, *120*, 167−193.

(6) Morrison, G. Modeling aqueous solutions near the critical point of water. *J. Solution Chem.* **1988**, *17*, 887−907.

(7) Penniger, J. M. L. Extraction of Oil from Wyoming Coal with Aqueous Solvents at Elevated Pressure. In *Supercritical Fluid Technology$* Penninger, J. M. L., Rodosz, M., McHugh, M. A., Krukonis, V. J., Eds.; Elsevier: New Yorkm 1987; pp 309−329.

(8) Modell, M. Supercritical water oxidation. *Chem. Phys. Processes Combust.* **1989**, E1−E7.

(9) Thomason, T. B.; Modell, M. Supercritical Water Destruction of Aqueous Wastes. *Haz. Wastes* **1984**, *1*, 453−467.

(10) Staszak, C. N.; Malinovski, K. C.; Killilea, W. R. The pilot-scale demonstration of the MODAR oxidation process for the destruction of hazardous organic waste materials. *Environ. Prog.* **1987**, *6*, 39−43.

(11) Shaw, R. V.; Brill, N. B.; Clifford, A. A.; Eckert, C. A.; Franck, E. U. Supercritical water: A medium for chemistry. *Chem. Eng. News* **1991**, *11*, 26−39.

(12) Barner, H. E.; Huang, C. Y.; Johnson, T.; Jacobs, G.; Martch, M. A. Supercritical water oxidation: An emerging technology. *J. Haz. Mater.* **1992**, *32*, 1.

(13) Helling, R. K.; Tester, J. W. Oxidation of simple compounds and mixtures in supercritical water: Carbon monoxide, Ammonia, and Ethanol. *Environ. Sci. Technol.* **1988**, *22*, 1319−1324.

(14) Houser, T. J.; Ying Zhou, Xu Liu. The destruction of selected hazardous compounds using supercritical water. *J. Supercrit. Fluids* **1996**, *9*, 106−112.

(15) Chialvo, A. A.; Cummings, P. T.; Kalyuzhnyi, Yu. V. Solvation effect on kinetic rate constant of reactions in supercritical solvents. *AIChE J.* **1998**, *44*, 667−680.

(16) Savage, P. E.; Gopalan, S.; Mizan, T. I.; Martino, J. C., Brock, E. E. Reactions at supercritical conditions: Applications and Fundamentals. *AIChE J.* **1995**, *41*, 1723−1778.

(17) Brennecke, J. F.; Chateauneuf, J. E. Homogeneous organic reactions as mechanistic probes in supercritical fluids. *Chem. Rev.* **1999**, *99*, 433−452.

(18) Savage, P. E. Organic chemical reactions in supercritical water. *Chem. Rev.* **1999**, *99*, 603−621.

(19) Hawthorne, S. B.; Yang, Y.; Miller, D. J. Extraction of organic pollutants from environmental solids with sub- and supercritical water. *Anal. Chem.* **1994**, *66*, 2912−2920.

(20) Yang, Yu.; Bowadt, S.; Hawthorne, S. B.; Miller, D. J. Subcritical water extraction of polychlorinated biphenyls from soil and sediment. *Anal. Chem.* **1995**, *67*, 4571−4576.

(21) Rebert, C. J.; Hayworth, K. E. The gas and liquid solubility relations in hydrocarbon−water systems. *AJChE J.* **1967**, *13*, 118−121.

(22) Connolly, J. F. Solubility of hydrocarbons in water near the critical solution temperatures. *J. Chem. Eng. Data* **1966**, *11*, 13−16.

(23) Rebert, C. J.; Kay, W. B. The phase behavior and solubility relations of the benzene−water system. *AIChE J.* **1959**, *5*, 285−289.

(24) Alwani, Z.; Schneider, G. M. Phasengleichgewichte, kritische erscheinungen und *PVT*-daten in binären mischungen von wasser mit aromatischen kohlenwasserstoffen bis 420 °C und 2200 bar. *Ber. Bunsen-Ges. Phys. Chem.* **1967**, *73*, 294−301.

(25) Bröllos, K.; Peter, K.; Schneider, G. M. Fluide mischsysteme unter hohem druck. Phasengleichgewichte und kritische Erscheinungen in den binären systemen cyclohexan-H_2O, *n*-heptan- H_2O und benzol- D_2O bis 420 °C und 3000 bar. *Ber. Bunsen-Ges. Phys. Chem.* **1970**, *74*, 682−686.

(26) Eckert, C. A.; Ziger, D. H.; Johnston, K. P.; Ellison, T. K. The use of partial molar volume data to evaluate equations of state for supercritical fluids mixtures. *Fluid Phase Equilib.* **1983**, *14*, 167−175.

(27) Zagrobelny, J.; Bright, F. V. Influence of solute-fluid clustering on the photophysics of pyrene emission in supercritical C_2H_4 and CF_3H. *J. Am. Chem. Soc.* **1992**, *114*, 7821−7826.

(28) Chialvo, A. A.; Cummings, P. T. Microstructure of ambient and supercritical water. Direct comparison between simulation and neutron scattering experiments. *J. Phys. Chem.* **1996**, *100*, 1309−1316.

(29) Londono, J. D.; Shah, V. M.; Wignall, G. D.; Cochran, H. D.; Bienkowski, P. R. Small angle neutron scattering studies of dilute supercritical solutions. I. Pure supercritical neon. *J. Chem. Phys.* **1993**, *99*, 466−470.

(30) Morita, T.; Nishikawa, K.; Takematsu, M.; Iida, H.; Furutaka, S. Structure study of supercritical CO_2 near high-order phase transition line by X-ray diffraction. *J. Phys. Chem. B* **1997**, *101*, 7158−7162.

(31) Nishikawa, K.; Morita, T. Small-angle X-ray scattering study of supercritical trifluoromethane. *J. Phys. Chem. B* **1997**, *101*, 1413−1418.

(32) Gao, J. Supercritical hydration of organic compounds. The potential of mean force for benzene in supercritical water. *J. Am. Chem. Soc.* **1993**, *115*, 6893−6895.

(33) Cummings, P. T.; Chialvo, A. A.; Cochran, H. D. Molecular simulation study of solvation structure in supercritical aqueous solutions. *Chem. Eng. Sci.* **1994**, *49*, 2735−2748.

(34) Cummings, P. T.; Chialvo, A. A. Molecular-based modeling of water and aqueous solutions at supercritical conditions. *Adv. Chem. Phys.* **1999**, *109*, 115.

(35) Chialvo, A. A.; Debenedetti, P. G. Molecular dynamics study of solute−solvent microstructure in attractive and repulsive supercritical mixtures. *Ind. Eng. Chem. Res.* **1992**, *31*, 1391−1397.

(36) Tucker, S. C.; Maddox, M. W. The effect of solvent density inhomogeneities on solute dynamics in supercritical fluids. *J. Phys. Chem. B* **1998**, *102*, 2437−2453.

(37) Panagiotopolos, A. Z. Direct determination of phase coexistence properties of fluids by Monte Carlo simulation in a new ensemble. *Mol. Phys.* **1987**, *61*, 813−826.

(38) Stapleton, M. R.; Tildeley, D. J.; Panagiotopolos, A. Z. Phase equilibria of quadrupolar fluids by simulation in the Gibbs ensemble. *Mol. Simulation* **1989**, *2*, 147−162.

(39) Amirkhanov, Kh. I.; Stepanov, G. V.; Abdulagatov, I. M.; Bouy, O. A. *Isochoric Heat Capacity of 1-Propanol and 2-Propanol*; DagFAN SSSR: Makhachkala, 1989.

(40) Kamilov, I. K.; Malysheva, L. V.; Rasulov, A. R.; Shakhbanov, K. A.; Stepanov, G. V. The experimental investigation of C_{VX}, *P*, *V*, *T* properties and the equation of state of the *n*-hexane−water system. *Fluid Phase Equilib.* **1996**, *125*, 177−184.

(41) Kamilov, I. K.; Stepanov, G. V.; Malysheva, L. V.; Rasulov, A. R.; Rasulov, S. M.; Shakhbanov, K. A. Phase equilibrium curves and critical lines of *n*-hexane−water: liquid−liquid and liquid−gas. *High Temp.−High Pressures* **1997**, *29*, 491−495.

(42) Stepanov, G. V.; Shakhbanov, K. A.; Malysheva, L. V. The thermodynamic properties of water−*n*-hexane mixture at critical and supercritical parameters. *Russ. High Temp.* **1997**, *35*, 192−197.

(43) Amirkhanov, Kh. I.; Abdulagatov, I. M.; Alibekov, B. G.; Stepanov, G. V.; Bou, O. A. Equation of state and thermodynamic properties of propan-2-ol. *J. Chem. Thermodyn.* **1988**, *20*, 513−522.

(44) Abdulagatov, I. M.; Stepanov, G. V.; Bou, O. A. Equation of state and thermodynamic properties of propan-1-ol. *J. Chem. Thermodyn.* **1991**, *23*, 617−627.

(45) De Loos, Th. W.; van Dorp, J. H.; Lichtenthaler, R. N. Phase equilibria and critical phenomena in fluid (*n*-alkane + water) systems at high pressures and temperatures. *Fluid Phase Equilib.* **1983**, *10*, 279−287.

(46) De Loos, Th. W.; Penders, W. G.; Lichtenthaler, R. N. Phase equilibria and critical phenomena in fluid (*n*-hexane + water) at high pressures and temperatures. *J. Chem. Thermodyn.* **1982**, *14*, 83−91.

(47) Yiling, T.; Berger, Th. M.; Franck, E. U. High-pressure equilibria and critical curves of (water + *n*-butane) and (water + *n*-hexane) at temperatures to 700 K and pressures to 300 MPa. *J. Chem. Thermodyn.* **1991**, *23*, 105−112.

(48) Brunner, E. Fluid mixtures at high pressures. IX. Phase separation and critical phenomena in 23 (*n*-alkane + water) mixtures. *J. Chem. Thermodyn.* **1990**, *22*, 335−353.
(49) Abdulagatov, I. M.; Bazaev, A. R.; Ramazanova, A. E. *PVTx* measurements of aqueous mixtures at supercritical conditions. *Int. J. Thermophys.* **1993**, *14*, 231−250.
(50) Abdulagatov, I. M.; Bazaev, A. R.; Ramazanova, A. E. *PVTx* properties and virial coefficients of the water-*n*-hexane system. *Ber. Bunsen-Ges. Phys. Chem.* **1994**, *98*, 1596−1600.
(51) Abdulagatov, I. M.; Bazaev, A. R.; Bazaev, E. A.; Saidakhmedova, M. B.; Ramazanova, A. E. Excess, partial, and apparent molar volumes of *n*-alkanes in near- and supercritical water. *J. Solution Chem.* **1998**, *27*, 729−751.
(52) Abdulagatov, I. M.; Bazaev, A. R.; Ramazanova, A. E. *PVTx*-properties and virial coefficients of binary water + *n*-hexane system. *Russ. High Temp.* **1992**, *30*, 897−907.
(53) Abdulagatov, I. M.; Bazaev, E. A.; Bazaev, A. R.; Rabezkii, M. G. *PVTx* measurements for dilute water + *n*-hexane mixtures in the near-critical and supercritical regions. *J. Supercrit. Fluids.* **2001**, *19*, 219−237.
(54) Majer, V.; Degrange, S.; Sedlbauer, J. Temperature correlation of partial molar volumes of aqueous hydrocarbons at infinite dilution: test of equations. *Fluid Phase Equilib.* **1999**, *158*−*160*, 419−428.
(55) Tsonopoulos, C.; Wilson, G. M. High-temperature mutual solubilities of hydrocarbons and water. *AIChE J.* **1983**, *29*, 990−999.
(56) Wormald, C. J.; Colling, C. N.; Lancaster, N. M.; Sellars, A. J. *Gas Processors Association, Research Report RR-68*; Tulsa, OK, 1983.
(57) Wormald, C. J.; Lancaster, N. M. Excess enthalpies and cross-term second virial coefficients for mixtures containing water vapour. *J. Chem. Soc., Faraday Trans. 1* **1988**, *84*, 3141−3158.
(58) Wormald, C. J. Heats of mixing of water + hydrocarbons at high temperatures and pressures. *Ber. Bunsen-Ges. Phys. Chem.* **1984**, *88*, 826−834.
(59) Neichel, M.; Franck, E. U. Critical curve and phase equilibria of water + *n*-alkane binary systems to high pressures and temperatures. *J. Supercrit. Fluids* **1996**, *9*, 69−74.
(60) Haruki, M.; Yahiro, Y.; Higashi, H.; Arai, Y. Correlation of phase equilibria for water + hydrocarbon systems at high temperatures and pressures by cubic equation of state. *J. Chem. Eng. Jpn.* **1999**, *32*, 535−539.
(61) Haruki, M.; Iwai, Y.; Nagao, S.; Yahiro, Y.; Arai, Y.; Measurements and correlation of phase equilibria for water + hydrocarbon systems near the critical temperature and pressure of water. *Ind. Eng. Chem. Res.* **2000**, *39*, 4516−4520.
(62) Eubank, Ph. T.; Wu, Ch. H.; Alvarado, J. F. J.; Forero, A.; Beladi, M. K. Measurement and prediction of three-phase water/hydrocarbon equilibria. *Fluid Phase Equilib.* **1994**, *102*, 181−203.
(63) Amirkhanov, Kh. I.; Stepanov, G. V.; Alibekov, B. G. *Isochoric Heat Capacity of Water and Steam*; Amerind Publishing: New Delhi, India, 1974.
(64) Polikhronidi, N. G.; Abdulagatov, I. M.; Magee, J. W.; Batyrova, R. G. Isochoric heat capacity for toluene near phase transitions and the critical point. *J. Chem. Eng. Data* **2001**, *46*, 1064−1071.
(65) Polikhronidi, N. G.; Abdulagatov, I. M.; Magee, J. W.; Stepanov G. V. Isochoric heat capacity measurements for light and heavy water near the critical point. *Int. J. Thermophys.* **2001**, *22*, 189−200.
(66) Polikhronidi, N. G.; Abdulagatov, I. M.; Batyrova, R. G. Isochoric heat capacity measurements for metastable fluids. *Int. J. Thermophys.* **2001**, in press.
(67) Polikhronidi, N. G.; Batyrova, R. G.; Abdulagatov, I. M. Isochoric heat capacity measurements of nitrogen tetroxide system at temperatures between 410 and 484 K and pressures up to 35 MPa. *Fluid Phase Equilib.* **2000**, *175*, 153−174.
(68) Polikhronidi, N. G.; Batyrova, R. G.; Abdulagatov, I. M. Two-phase isochoric heat capacity measurements for nitrogen tetroxide in the critical region and Yang-Yang relation. *Int. J. Thermophys.* **2000**, *21*, 1073−1095.
(69) Zakar'yaev, Z. R. Ph.D. Thesis, Institute for Geothermal Research, Makhachkala, 1995.
(70) Bochkov, M. M. Ph.D. Thesis, High-Temperature Institute, Moscow, 1985.
(71) Vargaftik, N. B. *Handbook of Physical Properties of Liquids and Gases*, 2nd ed.; Hemisphere: New York, 1983.
(72) Amirkhanov, Kh. I.; Alibekov, B. G.; Vikhrov, D. I.; Mirskaya, V. A. *Isochoric Heat Capacity and Other Caloric Properties of n-Alkanes*; DagFAN USSR: Makhachkala, 1981.
(73) Wagner, W.; Pruss, A. New international formulation for the thermodynamic properties of ordinary water substance for general and scientific use. *J. Phys. Chem. Ref. Data* **2001**, to be submitted.
(74) Span, R. *Multiparameter Equations of State—An Accurate Source of Thermodynamic Property Data*; Springer: Berlin, Germany, 2000.
(75) Magee, J. W.; Deal, R. J.; Blanco; J. C. High-temperature adiabatic calorimeter for constant volume heat capacity measurements of compressed gases and liquids. *J. Res. NIST* **1998**, *103*, 63−75.
(76) Chashkin, Ya. R.; Smirnov, V. A.; Voronel, A. V. *Thermophysical Properties of Substances and Materials*; GSSSD: Moscow, 1970; Vol. 2, pp 139−145.
(77) Voronel, A. V. *Phase Transitions and Critical Phenomena*; Domb, C., Green, M. S., Eds.; Academic Press: London, U.K., 1974; Vol. 5, pp 343−394.
(78) Ambrose, D.; Tsonopoulos, C. Vapor−liquid critical properties of elements and compounds. 2. Normal alkanes. *J. Chem. Eng. Data* **1995**, *40*, 531−546.
(79) Scheffer, F. E. C. *Konikl. Akad. Wetenschap. Amsterdam* **1914**, *17*, 835.
(80) Roof, J. G. Three-phase critical point in hydrocarbon−water systems. *J. Chem. Eng. Data* **1970**, *15*, 301−303.
(81) Levelt Sengers, J. M. H.; Straub, J.; Watanabe, K.; Hill, P. G. Assessment of critical parameter values for H_2O and D_2O. *J. Phys. Chem. Ref. Data* **1985**, *14*, 193−207 (revised values, on ITS-90, can be found in: *Physical Chemistry of Aqueous Systems*; White, H. J., Sengers, J. V., Neumann, D. B., Bellows, J. C., Eds.; Begell House: New York, 1995; Appendix A101−A102).
(82) Anisimov, M. A. *Critical Phenomena in Liquids and Liquid Crystals*; Gordon and Breach: Philadelphia, PA, 1991.
(83) Anisimov, M. A.; Kiselev, S. B. Universal crossover approach to description of thermodynamic properties of fluids and fluid mixtures. *Sov. Technol. Rev. B. Thermophys. Part 2*; Scheindlin, A. S., Fortov, V. E., Eds.; Harwood Academic: New York, 1992.
(84) Anisimov, M. A.; Voronel, A. V.; Gorodetskii, E. E. Isomorphism of critical phenomena. *Sov. Phys. JETP* **1971**, *33*, 605−611.
(85) Kiselev, S. B. Scaled equation of state of single-component liquids and binary solutions in the critical region. *Russ. J. High Temp.* **1988**, *26*, 466−471.
(86) Kiselev, S. B.; Friend, D. G. Cubic crossover equation of state for mixtures. *Fluid Phase Equilib.* **1999**, *162*, 51−82.
(87) Anisimov, M. A.; Povodyrev, A. A.; Roseli, J. P.; Sengers, J. V.; Kiselev, S. B.; Friend, D. G. Critical amplitudes of H_2O and D_2O in the near vicinity of the critical point. *Proceedings of the 13th International Conference on the Properties of Water and Steam*; Tremaine, P. R., Hill, Ph. G., Irish, D. E., Balakrishnan, P. V., Eds.; NRC Research Press: Ottawa, Canada, 2000; pp 339−346.
(88) Sengers, J. V.; Levelt-Sengers, J. M. H. Thermodynamic behavior of fluids near the critical point. *Annu. Rev. Phys. Chem.* **1986**, *37*, 189−222.
(89) Kiselev S. B.; Ely, J. F.; Abdulagatov, I. M.; Bazaev, A. R.; Magee, J. W. Equation of state and thermodynamic properties of pure toluene and dilute aqueous toluene solutions in the critical and supercritical regions. *Ind. Eng. Chem. Res.* **2001**, in press.

Received for review April 26, 2001. Accepted August 14, 2001. I.M.A. thanks the Physical and Chemical Properties Division at the National Institute of Standards and Technology (NIST) for the opportunity to work as a Guest Researcher at NIST during the course of this research. The research was supported by Grant RFBR 00-02-1732.

JE010136S